Electronic density of states of semiconductor alloys from lattice-mismatched isovalent binary constituents

Z. Q. Li and W. Pötz
Department of Physics, University of Illinois, Chicago, Illinois 60680
(Received 6 January 1992)

We present a model of the electronic density of states (DOS) for a wide class of ternary and quaternary semiconductor alloys. Our approach is based on a large-cluster calculation using a semiempirical tight-binding model for the electronic structure. The microscopic lattice configuration is efficiently determined by a Keating potential for the strain energy. The electronic DOS is calculated numerically via the recursion method. Results are presented for $ZnSe_{1-x}Te_x$. It is shown that the strong band bowing observed for this material is due to pure compositional disorder and bond-angle fluctuations. Bond-length fluctuations are found to be of minor significance. Without any free, adjustable parameters for the alloy, our model is in quantitative agreement with experimental data on the composition dependence of the main energy gap.

I. INTRODUCTION

A sound understanding of ternary and quaternary semiconductor alloys is an important prerequisite for successful design and fabrication of a new generation of electronic devices. Combination of group-IV, III-V, and II-VI semiconductors of various energy gaps and lattice constants has allowed the creation of artificial semiconductors with band gaps ranging from below zero to several eV.[1,2] A large variety of optoelectronic devices which are based on these alloys has been built or proposed. Semiconductor lasers and infrared detectors are probably the most prominent examples. More recently, the diversity of material properties has been largely broadened by successful growth of high-quality materials from lattice-mismatched constituents, II-VI materials, as well as their incorporation into superlattices and quantum wells.

While a sound understanding of the electronic structure of pure group-IV, III-V, and, to a lesser extent II-VI materials can be claimed, the electronic structure of ternary and quaternary alloys is still under extensive investigation. The disorder which characterizes these alloys makes conventional band-structure calculations which rely on the Bloch-Floquet theorem and the use of crystallographic unit cells rather inconvenient. For *ab initio* and other expensive computational techniques, the size of supercells which can be handled numerically is too small to represent an alloy. Recently, methods have been proposed which may help to overcome this problem for *ab initio* calculations.[3] Next to the adoption of small-size supercells,[4] several other approximation techniques have been applied to disordered semiconductor systems. The simplest approximation is the virtual-crystal approximation (VCA) which artificially reintroduces the fcc unit cell by resorting to virtual atoms. The properties of the virtual atom on a certain lattice site are composition-weighted averages of the properties of all the atoms which may occupy this particular site. All other information about substitutional disorder, such as the signature of the atom which actually occupies the site, and the local environment of the atom is lost. This approximation has been made within a variety of band-structure models.[1(a),5]

Agreement between experimental data and VCA predictions for the composition dependence of the main energy gap is generally rather poor. We have shown previously for $Al_xGa_{1-x}As$ that the neglect of compositional disorder is fully responsible for the failure of the VCA to reproduce the experimental composition dependence of the main energy gap.[6] Moreover, whereas some of the macroscopic properties of the system scale linearly with composition, various experiments on ternary and quaternary semiconductors have clearly established the failure of the VCA. For example, anion-cation bond lengths are remarkably independent from composition ratios.[7] Consequently, the nearest-neighbor positions cannot be perfectly tetrahedral. This has been confirmed by ferroelectric behavior and chemical shifts of nuclear magnetic resonance.[8,9] Photoemission spectroscopy has revealed that the density of states of the valence bands contains the signature of individual atoms and their local environment.[10] There is experimental evidence that **k**-vector conservation is not fulfilled in semiconductor alloys.[11] Phonon spectra of ternary and quaternary alloys maintain optical phonon modes which can be associated with the constituents.[12] Finally, band edges of ternary and quaternary alloys show considerably stronger band tailing than their binary constituents.[13]

Alternative to the VCA, a (single-site) coherent-potential approximation (CPA) has been used.[14,15] It has been shown to lead to a considerably better account of compositional disorder for $Al_xGa_{1-x}As$ than the VCA.[16] A refined method which is, to some extent, capable of accounting for both on-site and off-site disorder is the molecular coherent-potential approximation (MCPA).[17] Essentially, the CPA accounts for site disorder but uses an average local site environment. The incorporation of angle variations and strain fields is somewhat tedious and

agreement with experimental band-structure data is frequently unimpressive.

Cluster calculations, which do not require the presence of periodicity in the structure, represent an alternative to large supercell band-structure calculations. Numerically feasible cluster sizes scale inversely with the level of sophistication adopted for the representation of the atoms. Unfortunately, rather large clusters of more than $30\times30\times30$ atoms are needed for a realistic representation of ternary or quaternary alloys.[6,18]

In this paper, we present an efficient and accurate method to calculate the local density of states (LDOS) and density of states (DOS) of ternary and quaternary semiconductors. Our approach does not rely on the VCA, CPA, or the adoption of small unit cells and is capable of handling any alloy formed from (lattice-mismatched) ZnS-structured isovalent semiconductors. It reliably accounts for the composition dependence of the main energy gap and reveals the origins of band bowing as a function of composition. In particular, one can separate the contributions from purely compositional disorder, bond-length and bond-angle fluctuations. It makes possible a reliable quantitative prediction of the band gap for a large class of tetrahedral semiconductor alloys, and band-gap engineering is given a microscopic foundation. This is achieved by the use of the sp^3s^* semiempirical tight-binding (TB) model and the d^{-2} scaling law to represent the atoms and interatomic bonds in the alloy. The efficiency of the sp^3s^* model allows the use of clusters which may contain more than 50 000 atoms and, therefore, provide a realistic representation of all possible local atomic configurations. The latter are efficiently obtained by means of a Keating potential to relax a lattice of given composition into a state of minimum strain energy.[19,20] The tight-binding parameters and the parameters in the Keating potential are adjusted to reproduce experimental band-structure data and the elastic properties of the constituents, respectively. With use of the experimental values for the band offset between the constituents to relate TB parameters for different materials to each other, there are no free adjustable parameters in this model of the alloy. The evaluation of diagonal elements of the Green's function (resolvent) associated with the cluster is most conveniently performed via the recursion method.[21] Contrary to the CPA, there is no need to introduce an effective medium as long as the cluster is sufficiently large. As this approach gives the LDOS, it provides a theoretical means to probe local details of the electronic structure of a system, including disordered materials, heterostructures, and defect complexes.[22] We have developed an efficient code to calculate Green's-function matrix elements via the recursion method. Approximately 95% of the code could be vectorized to ensure efficient computation on a supercomputer.

Our model is presented in Sec. II. In Sec. III we discuss numerical aspects of our calculations. Section IV is devoted to a study of $ZnSe_{1-x}Te_x$. This material is of interest because of its wide band gap which makes it a potential candidate for green-blue light emitting optical devices. Moreover, it has extremely strong band bowing which is remarkable because there is no direct-gap–indirect-gap transition in this alloy. The energy gap of the alloy between $x\approx0.3$ and $x<1$ lies below the gaps of the two constituents, ZnSe and ZnTe. The VCA totally fails to reproduce this feature which makes this material an ideal candidate for testing our approach and for studying the origins of strong band bowing, as well as the limitations of the VCA. Moreover, *s-p*-orbital based TB models are sometimes believed to be too simple to account for the properties of II-VI semiconductors. By comparison with experiment, we show that they can be used successfully for the present purpose. Summary and conclusions are presented in Sec. V.

II. MODEL

First, a perfect fcc cluster of finite size is selected which may either be truncated at its surface or subjected to periodic boundary conditions. According to the composition ratios x and y of an alloy $A_xB_{1-x}C_yD_{1-y}$, atoms A and B are placed onto the cation sites and atoms C and D are placed on the anion sites, either completely at random or according to some empirical occupation correlation function. Every atom is given a label and record is kept of the relative position and identity of its four nearest neighbors. Once an atom has been placed onto every lattice site, the lattice is relaxed into a state of lowest strain energy. Generally, the constituent materials will not be lattice matched, and so the local bonding environment will deviate from the perfect tetrahedral fcc configuration. The bond length between two atoms, say A and C, is quite insensitive to the environment into which this pair is put,[7] whereas the average bond length follows Vergard's law.[23] The fact that in ZnS- and diamond-structured semiconductors bond-stretching forces dominate over bond-bending forces is well represented by a Keating potential for the strain energy, for which we choose the form[20]

$$U_K=\tfrac{3}{16}\sum_{ij}\frac{\alpha_{ij}}{R_{ij}^2}(\mathbf{r}_{ij}\cdot\mathbf{r}_{ij}-\mathbf{R}_{ij}\cdot\mathbf{R}_{ij})^2 +\tfrac{3}{8}\sum_i\sum_{j<k}\frac{\beta_{jik}}{R_{ij}R_{ik}}(\mathbf{r}_{ij}\cdot\mathbf{r}_{ik}-\mathbf{R}_{ij}\cdot\mathbf{R}_{ik})^2 . \quad (1)$$

Here, R_{ij} and r_{ij}, respectively, are the ideal (binary) and actual bond lengths between atoms i and j. α_{ij} and β_{jik} are force constants which determine the rigidity of bond lengths and bond angles, respectively. This simplest approximation for the deformation energy in a covalent solid has been verified to accurately reproduce experimental data on the structural properties of semiconductor alloys.[8] By reconsidering every site repeatedly, we continuously relax the lattice from a perfect fcc structure into a fourfold coordinate network of minimum energy.

Next, we account for the electronic properties of the atoms and their bonds. In view of its efficiency and the need for large-cluster sizes, the present model for the (L)DOS is based on a semiempirical sp^3s^* tight-binding model.[24] It was originally designed to account for the band structure of (indirect) semiconductors, but has subsequently been applied to numerous other problems.[25]

Every atom is characterized by five basis states, one s, three p, and one s^* state. The latter is used to compensate for the neglect of more than nearest-neighbor coupling. The Hamiltonian is of the form

$$H=\sum_{k,\mu}\varepsilon_{k\mu}|k\mu\rangle\langle k\mu|+\sum_{k\mu,j\nu}v_{k\mu,j\nu}|k\mu\rangle\langle j\nu| , \quad (2)$$

where $\varepsilon_{k\mu}$ is on-site energy and $v_{k\mu,j\nu}$ is the overlap integral for two states $|k\mu\rangle$ and $|j\nu\rangle$ of nearest-neighbor lattice sites k and j.

The TB matrix elements for the alloy are found by first adjusting the TB parameters to reproduce the main features of the experimental bulk band structure of the constituent binary semiconductors, whereby special attention is paid to the vicinity of the main energy gap. The main flaw of the present model, perhaps, is that it does not account for spin-orbit effects. In particular, the valence-band maximum is threefold (sixfold, with spin) degenerate. This somewhat restricts the applicability of the present version of the model. However, attempts have been made to account for spin-orbit effects within TB models.[26]

As the TB parameters associated with an atom, in general, depend on the host material, we adopt the following procedure to determine their values for atoms in the alloy. First, the diagonal elements $\varepsilon_{k\mu}$ of the atoms of a given constituent are shifted by a common constant to reproduce the experimental value for the band offset at the interface with the other constituent(s). In this way, we empirically establish a common reference level for the diagonal elements of all the atoms involved in the alloy. Then, the on-site energy associated with a given cation A in the alloy, $\varepsilon_A(A_xB_{1-x}C_yD_{1-y})$, is determined according to

$$\varepsilon_A(A_xB_{1-x}C_yD_{1-y})=\tfrac{1}{4}[N_C\varepsilon_A(AC)+N_D\varepsilon_A(AD)] , \quad (3)$$

where $\varepsilon_A(AI)$ are on-site energies for atom A in material AI and N_I is the number of nearest neighbors I. We proceed similarly for anions.

Off-diagonal elements are determined in the following way. For bonds A-C, material AC values are used; for bonds B-D, material BD values are used. However, these off-diagonal elements are subsequently modified according to the d^{-2} scaling law to account for the actual bond lengths in the cluster.[27] Moreover, for overlap integrals we follow Ref. 28 to account for the bond angles

$$\begin{aligned} V_{ss}&=V_{ss\sigma} , \\ V_{sx}&=lV_{sp\sigma} , \\ V_{xx}&=l^2V_{pp\sigma}+(1-l^2)V_{pp\pi} , \\ V_{xy}&=lmV_{pp\sigma}-lmV_{pp\pi} , \\ V_{xz}&=lnV_{pp\sigma}-lnV_{pp\pi} , \\ &\vdots , \end{aligned} \quad (4)$$

where $l=\cos\theta_x$, $m=\cos\theta_y$, and $n=\cos\theta_z$ explicitly account for the direction of the bond relative to the x, y, and z axis, respectively.

This procedure associates with the cluster a TB Hamiltonian matrix of high dimension in terms of the basis functions $|l\mu\rangle$. The LDOS for a certain orbital $|l\mu\rangle$ is given by

$$n(E,l\mu)=-\frac{1}{\pi}\lim_{\delta\to 0+}\mathrm{Im}\langle l\mu|G(Z)|l\mu\rangle . \quad (5)$$

Here $Z=E+i\delta$ and G is the resolvent operator for the system characterized by the Hamiltonian H. The diagonal element of the Green's function is found by a basis transformation which renders the matrix H in tridiagonal form, whereby the orbital $|l\mu\rangle$ is selected as the first normalized basis state. This procedure is known as the recursion method or Lanczos method and has been extensively discussed in the literature.[21]

The resulting matrix formally represents a semi-infinite linear chain with nearest-neighbor coupling in terms of which the desired matrix element of the resolvent operator can be expressed in the form of a continued fraction

$$\langle l\mu|G(Z)|l\mu\rangle=\cfrac{1}{Z-a_0-\cfrac{b_1^2}{Z-a_1-\cfrac{b_2^2}{Z-a_2-\cfrac{b_3^2}{\ddots}}}} . \quad (6)$$

$\{a_n\}$ and $\{b_n\}$, respectively, are the diagonal and off-diagonal matrix elements of the linear-chain Hamiltonian.

III. NUMERICAL DETAILS

Our model was used to obtain the electronic DOS for $ZnSe_{1-x}Te_x$, which will be presented in the next section. In this section we discuss some of the general numerical details which were necessary to perform the calculations.

Owing to the computational efficiency of the Keating and sp^3s^* models, large clusters can be used within the present approach. In the calculations for $ZnSe_{1-x}Te_x$ we used about 55 000 atoms. It should be noted that somewhat smaller clusters are sufficient to obtain a good representation of the overall band structure. However, for

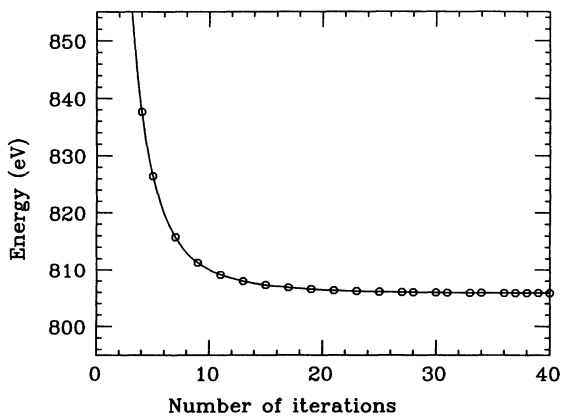

FIG. 1. Keating potential energy for $ZnSe_{0.6}Te_{0.4}$ vs number of iterations during the lattice relaxation.

TABLE I. Matrix elements of the tight-binding Hamiltonian in eV and bond length d in Å. a denotes the anion; and c, the cation.

	E_{sa}	E_{sc}	E_{pa}	E_{pc}	E_{s^*a}	E_{s^*c}	d (Å)
ZnSe	−13.131	2.151	0.114	7.216	7.588	8.924	2.454[a]
ZnTe	−11.017	0.912	0.935	5.665	7.179	8.368	2.643[a]
	V_{ss}	$V_{sp\sigma}$	$V_{ps\sigma}$	$V_{pp\pi}$	$V_{pp\sigma}$	$V_{s^*p\sigma}$	$V_{ps^*\sigma}$
ZnSe	−0.817	0.514	2.750	−0.908	2.497	1.255	2.830
ZnTe	−1.476	1.373	2.608	−0.610	2.947	1.269	2.179

[a]Reference 2(b).

an accurate representation of the density of states near the band edges, cluster sizes as used have been found necessary. Moreover, surface effects become negligible. In particular, we confirmed that whether the cluster is simply truncated or periodic boundary conditions are used does not influence the numerical results. In our calculations, we resorted to periodic boundary conditions. Every atom in the cluster is given a number and the labels and relative positions of next-nearest neighbors are recorded. In the present calculations, we started with a fcc lattice with the bond length determined by Vegard's law. Other initial configurations were used during the testing phase of the relaxation routine and convergence was achieved for any reasonable initial guess. Every atom of the cluster is repeatedly considered and relaxed into a position which minimizes the Keating energy of its vicinity, including up to next-nearest neighbors. Values for the force constants α and β which enter the Keating expression were taken from Ref. 20. We used $\alpha_{\mathrm{ZnTe}}=31.35$, $\beta_{\mathrm{TeZnTe}}=4.45$ and $\alpha_{\mathrm{ZnSe}}=35.24$, $\beta_{\mathrm{SeZnSe}}=4.23$ (all in units of N/m). For the Te-Zn-Se bond angle, the value $\beta_{\mathrm{SeZnTe}}=(\beta_{\mathrm{SeZnSe}}\beta_{\mathrm{TeZnTe}})^{1/2}=4.34$ N/m has been used. We found that typically 40 complete iteration cycles are required to achieve convergence within 0.1% for our cluster size. The relaxation code is largely sequential and takes about one hour of CPU time on Urbana's Cray Y-MP supercomputer. A typical run is plotted in Fig. 1.

The TB parameters of the sp^3s^* model for the constitutent materials were obtained by a fit to the lastest experimental data and, for some symmetry points, theoretical predictions. The main emphasis was put on an accurate description of the band structure in the vicinity of the main energy gap. The TB parameters used for ZnTe and ZnSe are listed in Table I. The energies at special symmetry points and a comparison to experimental and theoretical data are given in Table II. It can be seen that generally rather good agreement with experimental data

TABLE II. Comparison between theoretical band-structure calculations [nonlocal pseudopotential method (NLPM), linear combination of Gaussian orbitals (LCGO), modified orthogonalized plane wave (MOPW), and orthogonalized linear combination of atomic orbitals (OLCAO)] and experiment. Energies are in eV and relative to the Γ_{15}^v valence-band edge.

	ZnSe				ZnTe			
	Present work	NLPM[a]	LCGO[b]	Expt.	Present work	MOPW[c]	OLCAO[d]	Expt.
Γ_1^c	2.82	2.76	1.83	2.82[e]	2.394	2.6	2.39	2.394[f]
Γ_1^v	−13.8	−12.25	−12.67	−15.2[a]	−12.5	−10.8	−11.2	−13.0[g]
Γ_{15}^c	7.33	7.33			6.6	6.6	6.02	
X_1^v	−13.2	−10.72	−11.55	−12.5[g]	−11.62	−10.7	−9.81	−11.6[g]
X_3^v	−6.99	−4.96	−4.69	−5.3[h]	−6.04	−3.5	−4.29	−5.5[g]
				5.25[i]				
				5.6[g]				
X_5^v	−2.10	−1.96	−2.16	−2.1[g]	−2.0	−1.3	−1.92	−2.4[g]
				−2.5[i]				
X_1^c	4.54	4.54		4.3[j]	3.8	3.8	3.01	
X_3^c	4.82	5.71		5.1[j]	4.5	4.5	5.07	
L_1^v	−13.37	−11.08	−11.83	−13.1[g]	−11.86	−12.0	−10.16	−10.0[g]
L_1^v	−6.59	−5.08	−5.15	−5.6[g]	−5.65		−4.7	−5.5[g]
				−5.7[i]				
L_3^v	−0.81	−1.04	−0.85	−1.3[g]	−0.94	−0.5	−0.69	−1.1[g]
L_1^c	3.92	3.96		3.7[j]	3.44	3.4	3.39	

[a]Reference 29.
[b]Reference 30.
[c]Reference 36.
[d]Reference 37.
[e]Reference 31.
[f]Reference 38.
[g]Reference 32.
[h]Reference 33.
[i]Reference 34.
[j]Reference 35.

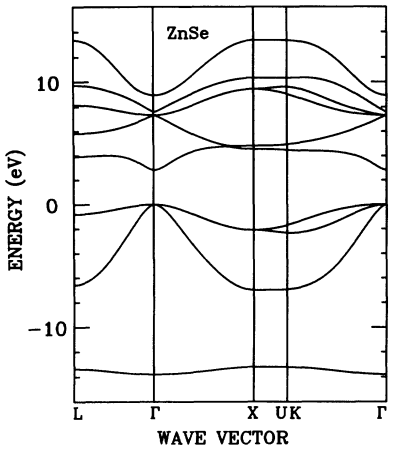

FIG. 2. The band structure for ZnSe as obtained from the sp^3s^* model.

can be achieved. It is well known that if all TB parameters are obtained by rigorously fitting experimental data for the valence bands, the lower conduction bands exhibit too little dispersion.[27] Some compromise had to be made for ZnSe, where accuracy at X_1^v and X_3^v was somewhat scarified in favor of a better fit for the lowest conduction bands. Nevertheless, our fit to experimental data compares favorably with various other band-structure calculations. The band structures of ZnSe and ZnTe as used in this study are given in Figs. 2 and 3, for completeness.

If there are N atoms in the cluster with five basis states per atom, the Hamiltonian operator is represented in the form of a $5N \times 5N$ matrix which is then subjected to the recursion method. We found that, for an accurate representation of the LDOS, typically 800 new basis states are sufficient. Thus we approximate a chain of $N \approx 55\,000$ sites by merely the first 800 sites. The continued fraction expression for the Green's function is simply truncated and evaluated numerically as a function of energy. Due to the cluster size, no terminator needs to be constructed. The value of δ in Eqs. (5) and (6) was chosen by comparison between the results for a virtual-crystal *cluster* and the corresponding VCA *band structure*. We found that $\delta \approx 10^{-2}$ eV is ideal for a representation of the overall density of states. The precise location of the band edges is best determined with $\delta \approx 10^{-6}$ eV. Here, we define the band gap as the energy separation between the uppermost valence-band level and the lowest conduction-band level of the cluster.

The recursion method actually gives the LDOS for a given basis state $|l\mu\rangle$, so we have to average over a large number of basis states to obtain the DOS. Here, we randomly pick approximately 20 pairs of atoms and average over the LDOS associated with all orbitals.

IV. RESULTS FOR $ZnSe_{1-x}Te_x$

We applied this model to $ZnSe_{1-x}Te_x$ because of its technological importance, as well as its interesting physical properties. The latter mainly concern the strong bowing of the main energy gap. Obviously, here we are dealing with a system which cannot be described within the VCA and subjects our approach to a critical test. One of our incentives here is to identify the origins of the discrepancies between experiment and VCA results. By a comparison with experimental data, we will verify that the approach outlined in Secs. II and III is capable of giving a realistic description of the DOS of semiconductor alloys, in particular, concerning the main band gap and its dependence on alloy composition.

We set the valence-band offset at the ZnTe-ZnSe type-II interface equal to 1.08 eV, consistent with experimental and theoretical data.[39] This is the only empirical parameter in the model which is not a bulk property. In principle, one should use the band offset for the interface of an unstrained ZnSe and an unstrained ZnSe interface. However, strain effects can be estimated to modify the valence-band offset by less than 10%, which is below the experimental accuracy. Moreover, we found that a change in the valence-band offset by 10% does not change our results noticeably.

We evaluated the DOS for $x = 0.2$, 0.4, 0.6, and 0.8. The DOS obtained from our method is given in Figs. 4–7 (solid lines) and compared to the results from the VCA (dotted lines). The latter was obtained by application of the recursion method to an ideal fcc lattice of virtual atoms, with the lattice constant determined by Vegard's

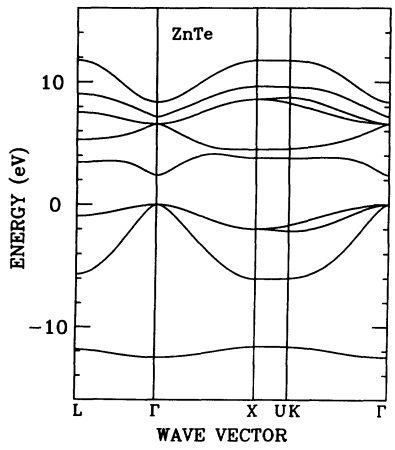

FIG. 3. The band structure for ZnTe as obtained from the sp^3s^* model.

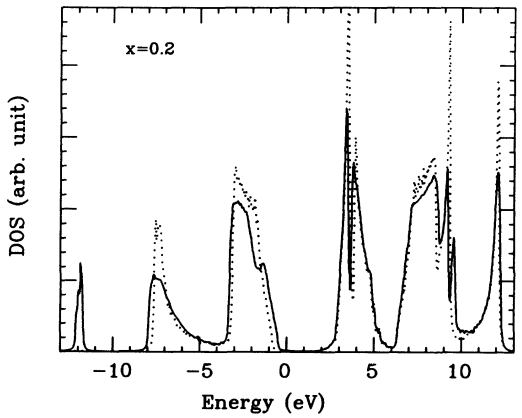

FIG. 4. The DOS for $ZnSe_{0.8}Te_{0.2}$. Dotted line, VCA; solid line, cluster calculation.

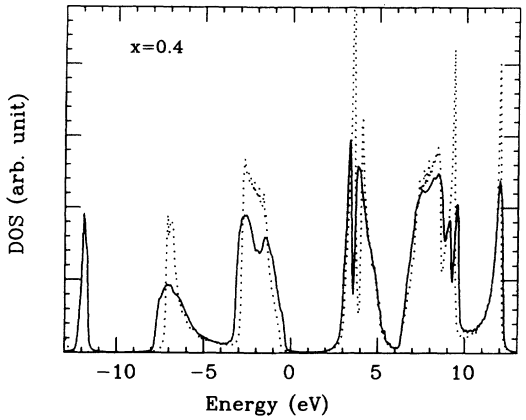

FIG. 5. Same as Fig. 4, for $ZnSe_{0.6}Te_{0.4}$.

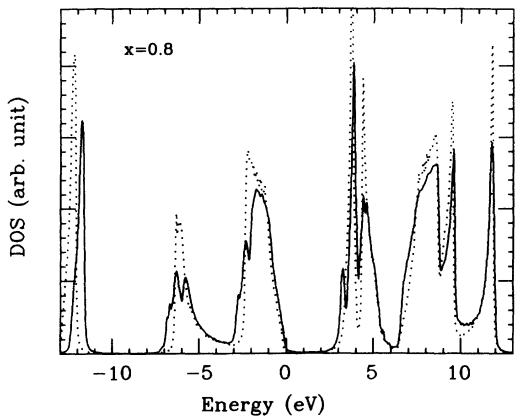

FIG. 7. Same as Fig. 4, for $ZnSe_{0.2}Te_{0.8}$.

law. The zero in the energy scale is at the valence-band edge of ZnTe. Figures 4–7 show that the broadening of the valence bands is clearly stronger than that of the conduction bands, which is consistent with CPA results and physical intuition:[17] conduction-band wave functions are less centered around atoms than valence-band wave functions and thus are less subject to effects of local disorder. The VCA generally predicts bands that are too narrow. Even more pronounced than a previous calculation for $Al_xGa_{1-x}As$,[6] the DOS, as obtained within the VCA, is significantly higher than predicted by our cluster calculation.

Moreover, the VCA overlooks essential features in the density of states by replacing the contributions of the Zn-Se and Zn-Te bonds by a single Zn-$(Se_{1-x}Te_x)$-bond contribution. Not shown in Figs. 4–7, the two lowest conduction bands, due mainly to Se and Te s states, are approximated by one band only. Moreover, the disappearing of the contribution of the Zn-Se bonds to the upper valence-band edge is overestimated and gives rise to a band gap which is too wide for $x \leq 0.5$ (Figs. 4 and 5). Similarly, for $x > 0.5$, only one peak accounts for the Zn-anion contribution to the lower conduction-band edge, whereas the cluster calculation gives two peaks centered around the single VCA peak. This provides an important contribution to the overestimation of the main energy gap for $x > 0.5$.

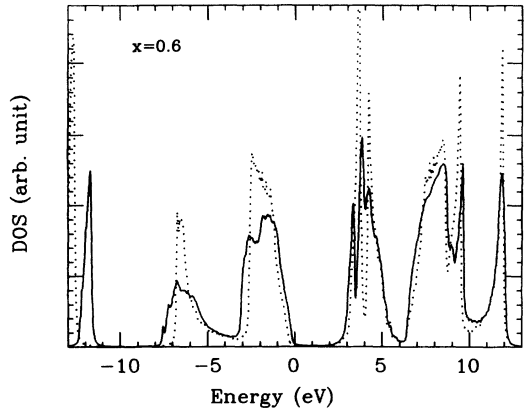

FIG. 6. Same as Fig. 4, for $ZnSe_{0.4}Te_{0.6}$.

In Fig. 8, the s, p, and s^* contributions per cation-anion pair to the DOS are shown for $x = 0.4$. It shows that, due to the hybridization between orbitals, the broadening of the bands is equally shared by the three different atomic orbitals. Again it is evident that the VCA gives single peaks, where the cluster calculation gives two. The lowest VCA valence band (not shown here), predominantly related to the anions s orbital, splits when disorder is accounted for, while the top valence band strongly broadens at the lower band edge and, to a lesser extent at the upper band edge. Additional features are clearly resolved in the upper valence band and in the conduction bands.

The experimental composition dependence of the main energy gap,[40] solid line in Fig. 9, can be well reproduced within the present approach (triangles), while the VCA (dotted line) fails to account for the strong bowing in this system. Numerically, the position of the band edges can be determined within less than 0.05 eV accuracy, as indicated by the error bars in Fig. 9.

The discrepancy between the present microscopic approach and the VCA has two related origins. First, the anion site can be occupied either by Se or Te. This is re-

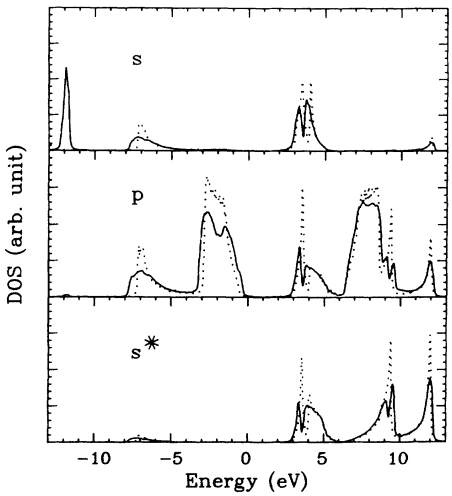

FIG. 8. Individual contributions to the DOS $ZnSe_{0.6}Te_{0.4}$ from s, p, and s^* orbitals.

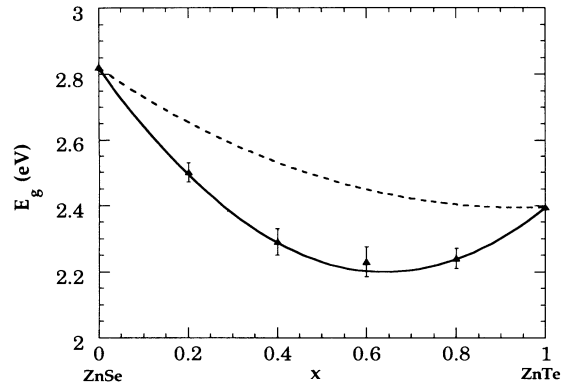

FIG. 9. The x dependence of the main energy gap of $ZnSe_{1-x}Te_x$. Dotted line: VCA; triangle with error bar: cluster calculation; solid line: experimental data (5 K) (Ref. 40).

ferred to as (purely) substitutional disorder. Second, nearest-neighbor bond lengths and bond angles may be different for every atom. We refer to this effect as bond-structure disorder. As for $Al_xGa_{1-x}As$, purely substitutional disorder must be expected to contribute to the widening of the bands. On the other hand, the large lattice mismatch of about 7% between ZnTe and ZnSe causes deviations from the perfect fcc lattice in the alloy. The local environment, i.e., the type of neighbors, of an atom determines the length and angles of its surrounding bonds. To determine the relative importance of substitutional disorder, bond-length and bond-angle fluctuations we considered $x=0.4, 0.6$ and calculated the DOS within four different versions of the model. The results near the top valence-band edge and the bottom of the conduction band are given in Figs. 10 and 11. The solid line refers to the method outlined in Secs. II and III and the dashed line gives the VCA result. The other two results were obtained by considering the same cluster but using TB parameters from the constituents without recalibration due to bond-length *and* bond-angle fluctuations (dotted line) and without recalibration due to bond-angle fluctuations, only (dot-dashed line).

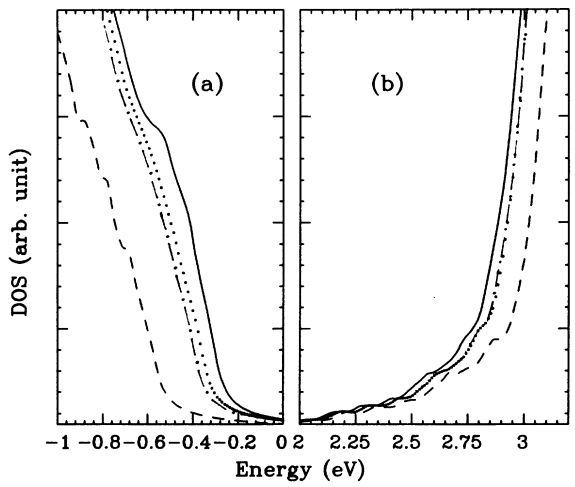

FIG. 10. The DOS in the vicinity of the gap for $ZnSe_{0.6}Te_{0.4}$, (a) near the top of the valence band; (b) near the bottom of the conduction band. Solid line, full cluster calculation; dashed line, VCA; dotted line, no account for bond-length and bond-angle variations in TB parameters; dot-dashed line, no account for bond-angle variations in TB parameters.

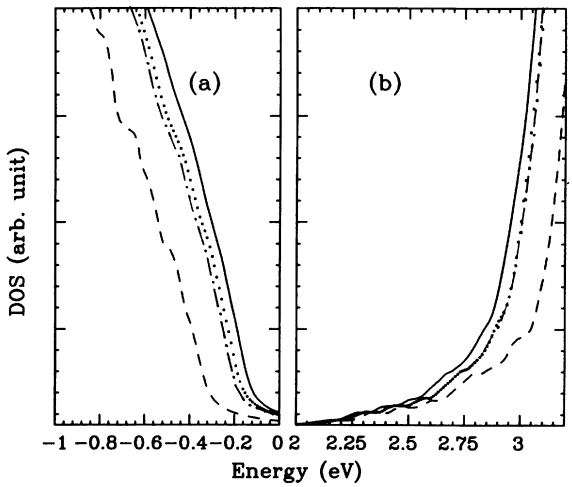

FIG. 11. Same as Fig. 10, for $ZnSe_{0.4}Te_{0.6}$.

A comparison with the VCA result shows that about three-quarters of the narrowing of the band gap is due to purely substitutional disorder, i.e., the fact that either a Te or Se atom occupies the anion site. This effect has formerly been shown to be entirely responsible for the discrepancy between the VCA band gap and experimental data for $Al_xGa_{1-x}As$.[6] Furthermore, the comparison reveals that bond-length fluctuations have a small effect on the band gap in the present case. In fact, here a slight widening is observed if the TB parameters are rescaled according to the d^{-2} law (dot-dashed line). Bond-angle fluctuations are found to account for the remaining $\leq 25\%$ of the band narrowing. Fixing the zero of energy at the valence-band edge of ZnTe and knowing the valence-band offset provide an absolute energy scale. Relative to the VCA result, the narrowing of the band gap arises from a broadening of both the conduction band and valence band as a function of x. Inspection of Figs. 4–7 shows that, for $x \leq 0.5$, the upward shift of the upper valence-band edge mainly contributes to the narrowing of the main energy gap. For instance, at $x=0.4$, Fig. 10, approximately 75% of the narrowing is due to a broadening of the valence-band edge. For $x>0.5$, the downward shift of the lower conduction-band edge gains in importance. Figure 11 shows that at $x=0.6$ conduction- and valence-band broadening have approximately equal importance for the narrowing of the gap. This trend can qualitatively be explained by considering the type-II band offset at the ZnSe-ZnTe interface. The valence-band edge of ZnSe lies about 1 eV below the valence-band edge of ZnTe. Consequently, the conduction band of ZnSe lies about 0.6 eV below the conduction-band edge of ZnTe. As the Te concentration is increased from $x=0$, Zn-Te bonds start to contribute to an increase in the density of states above the ZnSe valence-band edge, as well as a decrease in the density of states at the conduction-band edge of ZnSe due to a loss in ZnSe bonds. Conversely, substituting Te in ZnTe by

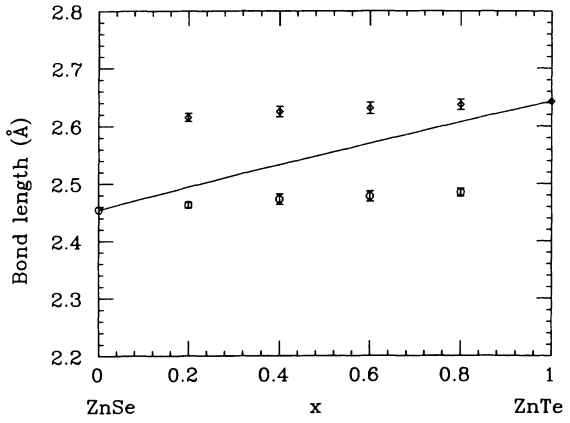

FIG. 12. The x dependence of the bond lengths in the relaxed cluster. Solid line, average bond length; diamonds, average length of Zn-Te bonds; circles, average length of Zn-Se bonds.

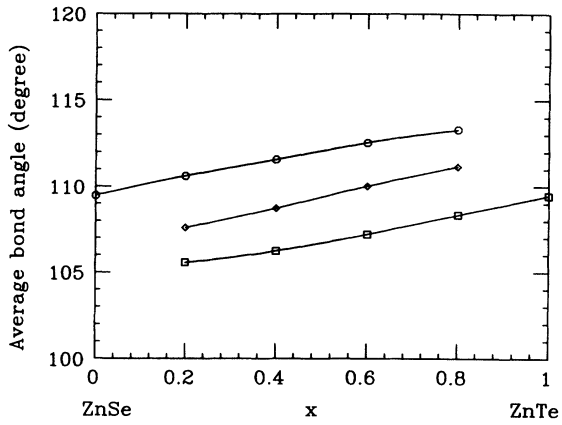

FIG. 14. The x dependence of the average Se-Zn-Se (circles), Zn-Te-Se (diamonds), and Te-Zn-Te (squares) bond angles. The solid lines serve as a guide to the eye.

Se provides energy levels below the ZnTe conduction-band edge. While these features are qualitatively correctly accounted for within the VCA, the latter neglects the individual signature of the anions and, as discussed above, approximates pairs of peaks due to the Zn-Se and Zn-Te bonds by a single Zn-$(Se_{1-x}Te_x)$-bond peak.

Finally, strain-induced changes in the local atomic environment, as obtained within the present model, should be discussed. The x dependence of bond lengths is displayed in Fig. 12. The average bond length of the relaxed cluster is found to scale according to Vegard's law, while the ZnTe (diamonds) and ZnSe bond length (circles) are rather insensitive to composition. Bond-length fluctuations remain below ≤ 0.01 Å, as indicated by the error bars in Fig. 12. The standard deviation of the bond angles from the ideal tetrahedral value is given in Fig. 13. Its peak value of 3° is reached just below $x=0.5$. This small asymmetry is due to slightly smaller rigidity of the ZnSe bond angle.

A more detailed picture of the local environment can be obtained by considering specific types of bond angles and their fluctuations for individual bonds. Due to much larger resistance to bond stretching, as compared with bond bending, the minimizing of the energy is accomplished primarily via deviation from the ideal tetrahedral bond angle. Considering Zn sites, there are three different bond angles labeled TeZnTe, TeZnSe, and SeZnSe. The mean value for these angles, given in Fig. 14, display a nearly linear dependence on composition. Figure 14 shows that the average SeZnSe bond angle is always larger than the ideal tetrahedral angle, while the average TeZnTe bond angle lies below the ideal fcc value. This is consistent with Fig. 12. Relative to the VCA bond length, the Zn atoms are pulled towards the Se atoms and pushed away from the Te atoms. The SeZnTe bond angle depends on the preferred nearest neighbors of Zn atoms. For $x<0.5$, where Se atoms are preferred nearest neighbors, the average value is below the ideal fcc value. Conversely, for $x>0.5$ where Te is the preferred nearest neighbor of Zn, the average value lies above the ideal fcc value.

The standard deviation from the average bond angle is given in Fig. 15. In all three cases, it displays a slightly asymmetric $x(1-x)$ behavior which reflects the randomness with which anion sites are populated. Due to a

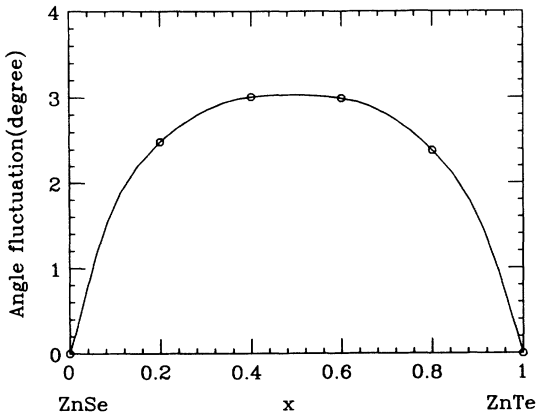

FIG. 13. The x dependence of the standard deviation of the bond angle from the ideal tetrahedral angle of 109.5°.

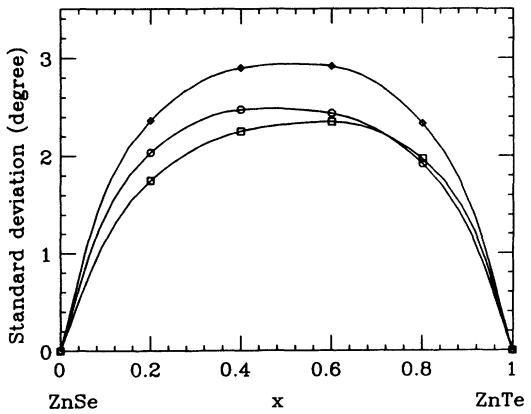

FIG. 15. The x dependence of the standard deviation from the average Se-Zn-Se (circles), Te-Zn-Se (diamonds), and Te-Zn-Te (squares) bond angles. The solid lines serve as a guide to the eye.

larger bond-angle stiffness in ZnTe, TeZnTe bond-angle fluctuations are slightly weaker than for the SeZnSe bond and peak at 2.3° and 2.5°, respectively. Slight asymmetries are due to next-nearest-neighbor effects. The largest bond-angle fluctuations are obtained for the SeZnTe bond angle, which reach a value of 3° around $x=0.5$.

V. SUMMARY AND CONCLUSIONS

We have presented an efficient method to calculate the electronic DOS for ternary and quaternary semiconductor alloys. Our approach is based on a large-cluster calculation which employs a Keating-type energy expression in conjunction with a semiempirical tight-binding model. The former is used to continuously relax the cluster from an ideal fcc structure to one of minimum strain energy. Based upon this relaxation, the TB parameters are determined using standard scaling laws. The TB matrix is then evaluated numerically within the recursion method to give the LDOS. An average over a large number of LDOS's is used to calculate the DOS in the vicinity of the main energy gap. This approach can be performed for any combination of isovalent binary semiconductors for which the Keating parameters and the TB binding parameters can be fitted to experiment and relativistic effects on the band structure are of minor significance. The (experimental) band offset(s) between the constituent materials is needed to properly shift the diagonal TB matrix elements.

Our calculations for $ZnSe_{1-x}Te_x$, and an earlier study of $Al_xGa_{1-x}As$, have shown that this approach leads to an accurate representation of the (L)DOS in very close agreement with experimental data. In particular, the composition dependence of the main energy gap is well reproduced. As compared to the virtual-crystal approximation, the energy bands get broadened at the expense of the band gaps and DOS within the bands. Additional structures which can be attributed to the signature of individual bonds are obtained. For $ZnSe_{1-x}Te_x$, our study attributes approximately 75% of the disorder induced narrowing of the main energy gap to a broadening of the band edges due to pure substitutional disorder. The remainder of the discrepancy is due to local strain effects caused by lattice mismatch. Here, bond-angle fluctuations are found to be clearly more important than bond-length fluctuations. Our calculations show that knowledge of the site which is substitutionally disordered cannot be used to identify the band edge which is most influenced by disorder. This is closely related to the failure of the "common-anion" rule for the band offset. Although the main contribution to the DOS at the top of the valence band and bottom of the conduction band may be attributed to anion p states and cation s states, respectively, the band edges which suffer most from disorder are determined by the band offset and the DOS associated with anion-cation bonds. The failure of the VCA for $ZnSe_{1-x}Te_x$ is therefore due to both a neglect of substitutional disorder and an incorrect account of local strain effects, in particular, bond-angle fluctuations.

In its present form, our model does not account for relativistic effects which are important for some semiconductors. In particular, the split-off band is not properly accounted for. Attempts to incorporate relativistic effects in TB-based band-structure calculations have been made and could be carried over to alloys.[26] Moreover, d levels are not explicitly accounted for in this model. Despite the fact that these levels may be important in *ab initio* band-structure calculations of certain semiconductors,[36] the empirical TB model is able to account for the main electronic properties of the alloys in the case of $Al_xGa_{1-x}As$ and $ZnSe_{1-x}Te_x$.

In summary, this work has demonstrated that quantitative information concerning the (L)DOS of ternary and quaternary semiconductor alloys can be made with use of this semiempirical model with a reasonable computational effort. It has been shown previously that this method can be used to investigate the LDOS in semiconductor quantum well structures with or without imperfections.[22] Application to defect complexes and amorphous semiconductor systems, their alloys, and heterostructures is possible.

ACKNOWLEDGMENTS

This work has been supported by the U.S. Army Research Office. Furthermore, we acknowledge support from the NSF via the National Center for Supercomputing Applications and the National Center for Computational Electronics, University of Illinois, Urbana-Champaign.

[1](a) M. Jaros, Rep. Prog. Phys. **48**, 1091 (1985); (b) *Physics and Application of Semiconductor Microstructures* (Oxford University Press, London, 1989).

[2](a) *Numerical Data and Functional Relationship in Sciences and Technology,* edited by O. Madelung, M. Schulz, and H. Weiss, Landolt-Börnstein, New Series, Vol. 17a,b (Springer-Verlag, Berlin, 1982); (b) *Semiconductors: Physics of II-VI and I-VII Compounds, Semimagnetic Semiconductors,* edited by O. Madelung, Landolt-Börnstein, New Series, Vol. 17b (Springer-Verlag, Berlin, 1987); *Semiconductors: Intrinsic Properties of Group Elements and III-V, II-VI and I-VII Compounds,* edited by O. Madelung, Landolt-Börnstein, New Series, Vol. 22a,b (Springer-Verlag, Berlin, 1987).

[3]A. Zunger, S.-H. Wei, L. G. Ferreira, and J. E. Bernard, Phys. Rev. Lett. **65**, 353 (1990); Rita Magri, Sverre Froyen, and Alex Zunger, Phys. Rev. B **44**, 7947 (1991).

[4]J. D. Joannopoulos and M. L. Cohen, Phys. Rev. B **8**, 2733 (1973).

[5]H. P. Hjalmarson, P. Vogl, D. J. Wolford, and J. D. Dow, Phys. Rev. Lett. **44**, 810 (1980).

[6]Z. Q. Li and W. Pötz, Phys. Rev. B **43**, 12 670 (1991).

[7]J. C. Mikkelson and J. B. Boyce, Phys. Rev. Lett. **49**, 1412 (1982); Phys. Rev. B **28**, 7130 (1983); H. Oyanagi, Y. Takedo, T. Matsushita, T. Ishiguro, T. Yao, and A. Sasaki, Solid State Commun. **67**, 453 (1988); A. Balzarotti, A. Kisiel, N. Motta, M. Zimnal-Starnawska, M. T. Czyżyk, and M. Podgòrny,

Phys. Rev. B **30**, 2295 (1984); T. Sasaki, T. Onda, and R. Ito, Jpn. J. Appl. Phys. **25**, 231 (1986); J. Bellessa, C. Gors, P. Launois, M. Quillec, and H. Launois, in *Gallium Arsenide and Related Compounds, 1982: Contributed Papers from the Tenth International Symposium on Gallium Arsenide and Related Compounds,* edited by G. Stillman, IOP Conf. Proc. No. 65 (Institute of Physics and Physical Society, London, 1983), Chap. 6, p. 529; N. Motta, A. Balzarotti, P. Letardi, A. Kisiel, M. T. Czyżk, M. Zimnal-Starnawska, and M. Podgòrny, Solid State Commun. **53**, 509 (1985); A. Marbeuf, D. Ballutaud, R. Triboulet, H. Dexpert, P. Lagarde, and Y. Marfaing, J. Phys. Chem. Solids **50**, 975 (1989).

[8]R. Weil, R. Nkum, E. Muranevich, and L. Benguigui, Phys. Rev. Lett. **62**, 2744 (1989).

[9]K. Beshah, D. Zamir, P. Becla, P. A. Wolff, and R. G. Griffin, Phys. Rev. B **36**, 6420 (1987); D. B. Zax, S. Vega, N. Yellin, and D. Zamir, Chem. Phys. Lett. **138**, 105 (1987).

[10]K. L. Tsang, J. E. Rowe, T. A. Callcott, and R. A. Logan, Phys. Rev. B **38**, 13 277 (1988).

[11]H. Kalt, W. W. Rühle, and K. Reimann, Solid-State Electron. **32**, 1819 (1989).

[12]See, for example, K. T. Tsen and H. Morkoç, Phys. Rev. B **37**, 7137 (1988); A. Kobayashi and A. Roy, *ibid.* **35**, 5611 (1987).

[13]S. John, C. Soukoulis, M. H. Cohen, and E. N. Economou, Phys. Rev. Lett. **57**, 1777 (1986).

[14]E. N. Economou, *Green's Functions in Quantum Physics* (Springer, Berlin, 1979).

[15]A.-B. Chen and A. Sher, Phys. Rev. Lett. **40**, 900 (1978).

[16]A.-B. Chen and A. Sher, Phys. Rev. B **23**, 5360 (1981); S. N. Grinyaev, S. G. Kataev, and V. A. Chaldysher, Izv. Vyssh. Uchebn. Zaved. Fiz. **29**, 514 (1986) [Sov. Phys. J. **29**, 514 (1986)].

[17]K. C. Hass, R. J. Lempert, and H. Ehrenreich, Phys. Rev. Lett. **52**, 77 (1984); R. J. Lempert, K. C. Hass, and H. Ehrenreich, Phys. Rev. B **36**, 1111 (1987).

[18]Mattias C. Schabel and José Luís Martins, Phys. Rev. B **43**, 11 873 (1991).

[19]P. N. Keating, Phys. Rev. **145**, 637 (1966).

[20]Richard M. Martin, Phys. Rev. B **1**, 4005 (1970).

[21]Roger Haydock, in *Solid State Physics: Advances in Research and Applications,* edited by Henry Ehrenreich, Frederick Seitz, and David Turnbull (Academic, New York, 1980); Vol. 35; *The Recursion Method and its Applications,* edited by D. G. Pettifor and D. L. Wearie, Springer Series in Solid-State Sciences Vol. 58 (Springer-Verlag, Berlin, 1985).

[22]Z. Q. Li and W. Pötz, J. Vac. Sci. Technol. B **9**, 2251 (1991).

[23]L. Vegard, Z. Phys. **5**, 17 (1921).

[24]P. Vogl, Harold P. Hjalmarson, and John D. Dow. J. Phys. Chem. Solids **44**, 365 (1983).

[25]For example, P. Vogl, in *Festkörperprobleme (Advances in Solid State Physics),* edited by J. Treusch (Vieweg, Braunschweig, 1981), Vol. 21, p. 191; Shang Yuang Ren, John D. Dow, and Jun Shen, Phys. Rev. B **38**, 10 677 (1988); E. P. O'Reilly and J. Robertson, *ibid.* **34**, 8684 (1986).

[26]D. J. Chadi, Phys. Rev. B **16**, 790 (1977).

[27]W. A. Harrison, *Electronic Structure and the Properties of Solids* (Freeman, San Francisco, 1980).

[28]J. C. Slater and G. F. Koster, Phys. Rev. **94**, 1409 (1954).

[29]J. R. Chelikowski and M. L. Cohen, Phys. Rev. B **14**, 556 (1976).

[30]C. S. Wang and M. M. Klein, Phys. Rev. B **24**, 3393 (1981).

[31]H. Venghaus, Phys. Rev. B **19**, 3071 (1979).

[32]L. Ley, R. A. Pollark, F. R. McFeely, S. P. Kowalczyk, and D. A. Shirley, Phys. Rev. B **9**, 600 (1974).

[33]D. E. Eastman, W. D. Grobman, J. L. Freeouf, and M. Erbudak, Phys. Rev. B **9**, 3473 (1974).

[34]A. Ebina, T. Unno, H. Suda, H. Koinuma, and T. Takahashi, J. Vac. Sci. Technol. **19**, 301 (1981).

[35]M. Cardona, J. Appl. Phys. Suppl. **32**, 2151 (1961).

[36]S. I. Kurganskii, O. V. Farberovich, and E. P. Domashevskaya, Fiz. Tekh. Poluprovodn. **14**, 1315 (1980) [Sov. Phys. Semicond. **14**, 775 (1980)]; **14**, 1412 (1980) [**14**, 837 (1980)].

[37]M. Z. Huang and W. Y. Ching, J. Phys. Chem. Solids **46**, 977 (1985).

[38]H. Venghaus and P. J. Dean, Phys. Rev. B **21**, 1596 (1980).

[39]Y. Rajakarunanayake, R. H. Miles, G. Y. Wu, and T. C. McGill, J. Vac. Sci. Technol B **6**, 1354 (1988); W. A. Harrison, J. Vac. Sci. Technol. **14**, 1016 (1977).

[40]M. J. S. P. Brasil, R. E. Nahory, F. S. Turco-Sandroff, H. L. Gilchrist, and R. J. Martin, Appl. Phys. Lett. **58**, 2509 (1991).